We are IntechOpen,
the world's leading publisher of
Open Access books
Built by scientists, for scientists

4,800
Open access books available

122,000
International authors and editors

135M
Downloads

Our authors are among the

154
Countries delivered to

TOP 1%
most cited scientists

12.2%
Contributors from top 500 universities

CLARIVATE ANALYTICS
BOOK CITATION INDEX
INDEXED

WEB OF SCIENCE™

Selection of our books indexed in the Book Citation Index
in Web of Science™ Core Collection (BKCI)

Interested in publishing with us?
Contact book.department@intechopen.com

Numbers displayed above are based on latest data collected.
For more information visit www.intechopen.com

Monte Carlo Simulation for Magnetic Domain Structure and Hysteresis Properties

Katsuhiko Yamaguchi, Kenji Suzuki and Osamu Nittono
Fukushima University
Japan

1. Introduction

Recently many studies for magnetic process simulations of micro magnetic clusters have been performed using several calculation methods. These studies are expected to be available to realize high-density magnetic memories, new micro-magnetic devices or to analyze microscopically for magnetic non destructive evaluation. Monte Carlo (MC) method is one of useful and powerful methods to simulate magnetic process for magnetic clusters including complicated interaction such as different exchange interactions due to different elements and to introduce magnetic properties depending on temperature.

To apply MC method for magnetic process simulation, there were some problems. One is that MC method is originally dealing with stable states, that is, the time processes on MC simulations can not be usually recognized as the real changes on time, e.g. for hysteresis curves (M-H curves) with increasing and decreasing applied magnetic field. Then a pseudo-dynamic process for MC method is introduced for dealing with such a simulation on section 2. Next problem is that the MC calculation for large clusters demands huge CPU time because it is necessary to repeat MC step (MCS) until N for the cluster cell number N. Especially the magnetic dipole interaction which is included in Hamiltonian must be calculated among all the spins in the cluster. Then a new technique of MC method by a parallelized program is introduced for dealing with larger cluster on section 3. The useful calculation results using these MC methods are presented on following sections. Section 4 introduces the producing of magnetic domains and domain walls (DWs) for the clusters including spins affected by exchange interaction, magnetic dipole interaction and crystal anisotropy. On section 5, magnetic domain wall displacements (DWDs) are shown for nano-wires with local magnetic impurity. On section 6, M-H curves are shown for magnetic clusters with a local magnetic distribution corresponding with grain boundary of Ni based alloy. For elementary theory on MC method, previous chapter should be referred.

2. Pseudo-dynamic process on MC method

In general, MC method deals with thermal equilibrium states. Therefore usually MC steps are repeated until getting a stable state. Here 1 MC step (MCS) means scanning up to the total cell number of times for the spin-flip process. Ordinary repeating MCS is set to N MCS,

here N is the total number of spin sites. But now we stopped the repeating before getting a stable state because of dealing with magnetic dynamic processes (Yamaguchi *et al*. 2004). Under the constant magnetic field condition, the total spin is in a non-equilibrium state and going to an equilibrium state with progressing MC steps. The magnetic field slightly increases before achievement of the equilibrium state, then the total spin is kept under another non-equilibrium state again and proceeding to a new equilibrium state as show Fig.1. The operation is renewed until achievement of final magnetic field. Because the change of the magnetic field is minute, it will be able to regard approximately that a series of steps is continuous process through a pseudo-non-equilibrium state. Here an assumption is introduced that magnetization intensity, namely the summation of total spin, of each MC step can reflect the magnetic dynamic process on magnetic hysteresis.

Pseudo-dynamic process on MC method is useful for dealing with magnetic dynamic simulation, e.g., magnetic hysteresis curves or magnetic domain wall moving, as they are explained in later sections.
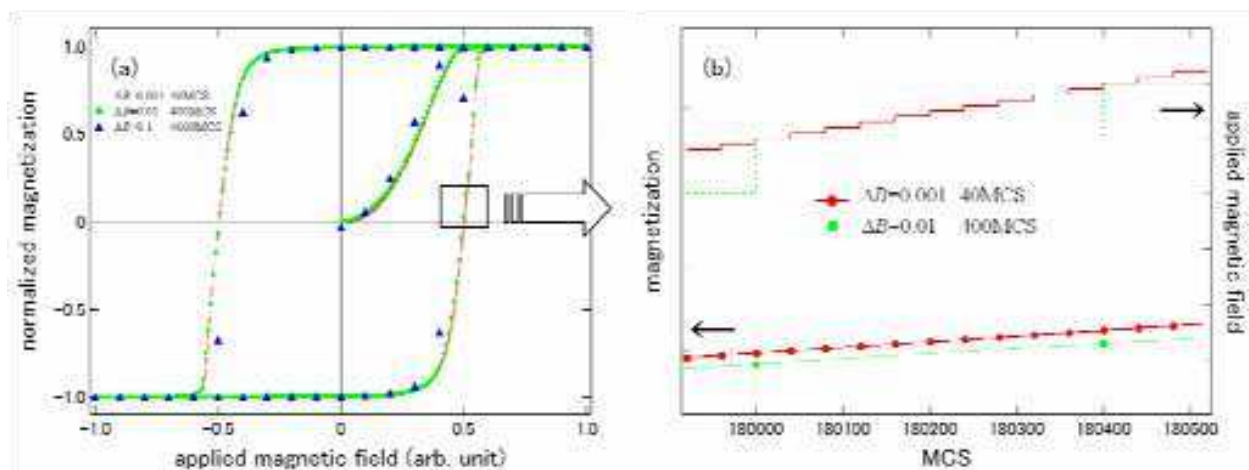

Fig. 1. (a) Magnetic hysiteresis curves for a cluster with different step of applied magnetic field ΔB. (b) Example of MC step dependence on applied magnetic field and magnetization. Circles show the last data of magnetization under the same condition.

3. Parallelized MC algorithm

In this section, for explanation of parallelized MC algorithm, a following Hamiltonian is used:

$$H = H_J + H_D + H_B$$
$$= -\sum_{near} J_{ij} \mathbf{S}_i \cdot \mathbf{S}_j + D\sum_{all}\left(\frac{\mathbf{S}_i \cdot \mathbf{S}_j}{\left|\mathbf{r}_{ij}\right|^3} - \frac{3}{\left|\mathbf{r}_{ij}\right|^5}\left(\mathbf{S}_i \cdot \mathbf{r}_{ij}\right)\left(\mathbf{S}_j \cdot \mathbf{r}_{ij}\right) \right) + B\sum_i \mathbf{S}_i . \tag{1}$$

H_J term, H_D term and H_B term represent exchange interaction energy, magnetic dipole interaction energy and applied magnetic field energy, respectively. Here $\mathbf{S}_i$ denotes the spin state of i-th cell and $\mathbf{r}_{ij}$ represents the distance between i-th spin and j-th spin. Below we deal with clusters with the lattice constant of 1 and this is regarded as a criterion of length. In the first term H_J, J_{ij} stands for an exchange interaction energy constant for i-th and j-th spins.

Usually exchange interaction works on only neighbor spins, because the interaction is originally due to overlapping between wave functions of electrons with spins, then the summation is limited to the extent in an effective radius r_{eff} from a target spin $\boldsymbol{S}_i : |\boldsymbol{r}_{ij}| \leq r_{eff}$. In the second term H_D, D for a magnetic dipole interaction constant for i-th and j-th spins. The magnetic dipole interaction works on all spins because it is due to magnetic field interspersed in all space. Then the summation includes the interaction energy between i-th spin and all j-th spins except for $j=i$. In the third term H_B, B represents applied magnetic field which acts equally all spins.

For parallelizing MC program, it is important to keep causality of MC algorithm. Hence it is not allowed that before a spin $\boldsymbol{S}_i$ is updated by MC process, the next calculation starts about another spin $\boldsymbol{S}_i'$. Therefore a feasible parallelized process is limited to the summation for a fixed $\boldsymbol{S}_i$. Then Eq.(1) was transformed for applying the parallelized algorithm to MC method without spoiling the causality as follows:

$$H = \sum_i \left\{ \sum_{j \neq i} \left[-J_{ij} \boldsymbol{S}_i \cdot \boldsymbol{S}_j \delta_{|i-j|,1} + D \left(\frac{\boldsymbol{S}_i \cdot \boldsymbol{S}_j}{|\boldsymbol{r}_{ij}|^3} - \frac{3}{|\boldsymbol{r}_{ij}|^5} (\boldsymbol{S}_i \cdot \boldsymbol{r}_j)(\boldsymbol{S}_j \cdot \boldsymbol{r}_j) \right) \right] + B\boldsymbol{S}_i \right\}. \tag{2}$$

Here the inner summation for j of Eq.(2) can be parallelized. Kronecker's δ limits the summation of j for the first term to the extent of the nearest neighbors (note r_{eff} =1 in this case) with checking the distance between i-th and j-th spins on each selection of a target spin $\boldsymbol{S}_i$. Although the check process adds a load for CPU power, the program parallelizing the summation of j in block is effective for larger clusters.

Figure 2 shows a flowchart of the MC algorithm including the parallelized process. After choosing a target spin $\boldsymbol{S}_i$ randomly under an initial state, all j-th spins except for $j=i$ are divided into plural CPU in a parallel computer. A CPU assigned to a set for $\boldsymbol{S}_i$ and $\boldsymbol{S}_j$ calculates $\boldsymbol{r}_{ij}$ and distinguishes $|\boldsymbol{r}_{ij}| \leq r_{eff}$ and $|\boldsymbol{r}_{ij}| > r_{eff}$. Note that $r_{eff} \geq 1$ is allowed in general. The CPU calculates H_J and H_D, and the summation of them is stocked into a memory with the results by other CPUs. This process is repeated until last j (=N) which is the total spin number of dealing cluster. After adding applied magnetic field energy H_B, the target spin $\boldsymbol{S}_i$ is updated by Metropolis method (Metropolis *et al.* 1953, Landau & Binder 2000). The update of $\boldsymbol{S}_i$ is repeating N times, that is, all spins are updated as an average. This period is called one MC step (1 MCS). For getting stable physical quantities, the calculation process is repeating M times (= M MCS) under the same condition. M sets usually N, therefore the parallelized process repeats N^2 times and the process is expected to reduce the calculation time. Using above algorithm, all simulations in this chapter were carried out by the use of the parallel super-computer, Altix3700B in the Institute of Fluid Science, Tohoku University (Japan).

Figure 3 shows the wall time (actual calculating time) during 1000 MCS repeating for different size squares with the one side length L=20, 30, 50, 75, 100 and 150 cells for each CPU number used in the same time. N (=L^2) is total cell number. The increase of CPU number effectively reduces the calculation time especially for larger clusters. The calculation results for the same cluster have no discrepancy among using of different CPU numbers.

Figure 4 shows the total CPU time and the wall time for the calculations for different size clusters at a fixed temperature. The numbers in brackets show the CPU numbers for each calculation.

Figure 5 shows results of temperature dependence of the normalized magnetization M for different size clusters. For clusters with the one side length between $L=10$ and 50, the results well obey the Curie-Weiss law and the Curie temperatures were estimated at about $k_B T_c=1.0$. For larger clusters, however, the increases of the magnetizations are not seen at low temperature.

In general it is known that closure domain structure of spin system appears for thin film magnetic cluster due to magnetic dipole interaction although single magnetic domain is produced for the smaller cluster (Sasaki & Matsubara 1997, Vedmedenko *et al.* 2000). Then above results of magnetization will be also size effect due to magnetic dipole interaction.
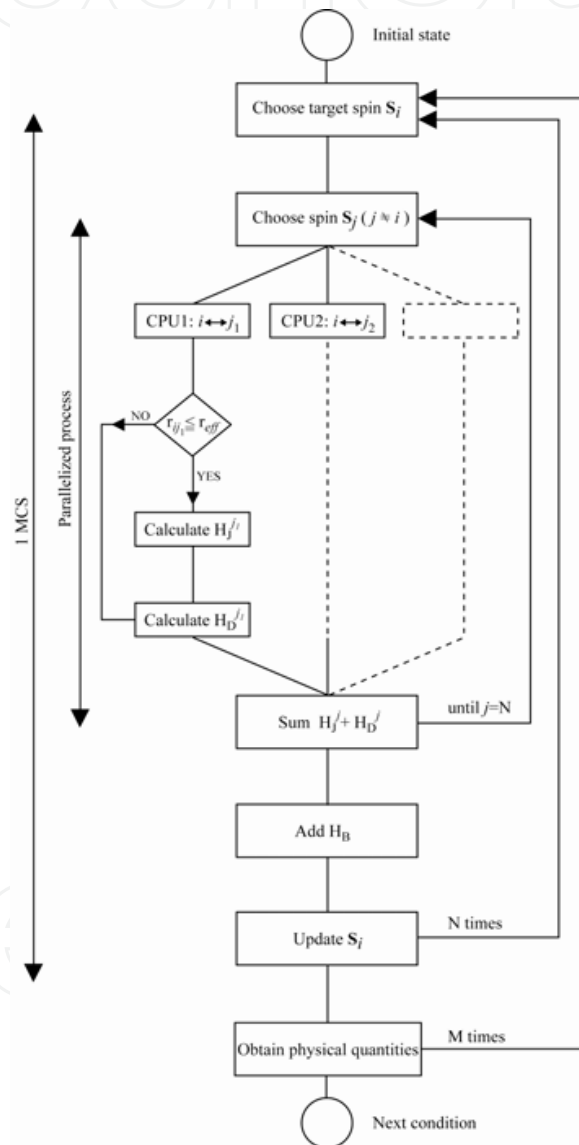
Fig. 2. Flowchart of MC algorithm including parallelized process. The process from "Choose spin S_j" to "Sum $H_J + H_D$" is parallelized in this algorithm. The process from "Choose spin S_i" to "Update S_i" is repeating until spin total number N and it is called 1MCS.

Figure 6 shows spin snapshots for the different size square clusters with the one side length of $L=10$, 50, 75, respectively at lowest temperature. It is clearly seen that the closure domain structure of spin system actually appears for the cluster with $L=75$.
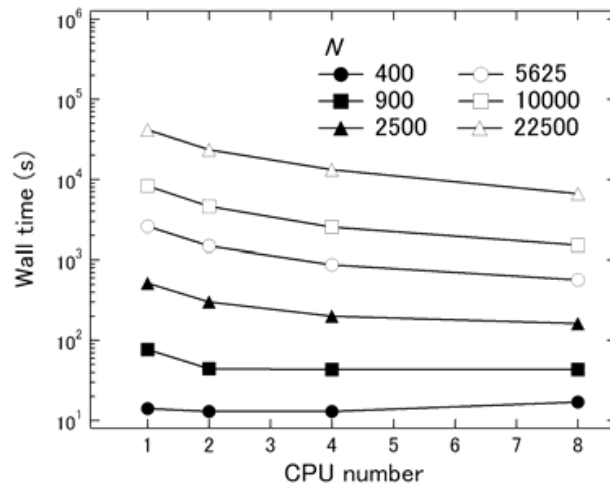
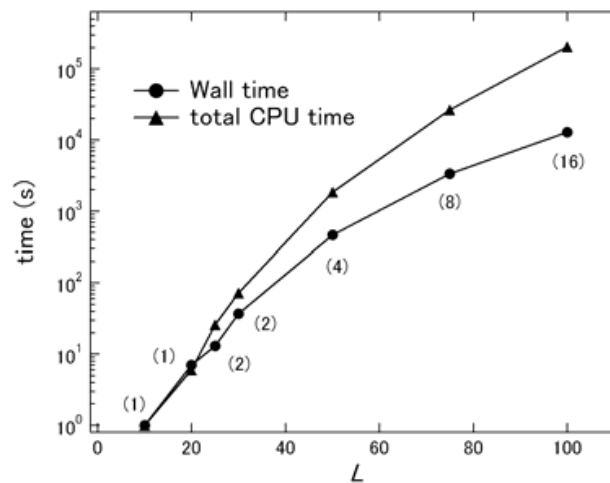Fig. 3. Wall time during 1000 MCS depending on CPU number for each size cluster ($N=L2$).

Fig. 4. Total CPU time and wall time on calculation at a fixed temperature for each size cluster. Numbers in brackets ( ) show the CPU numbers for parallel calculation.

The closure domain structure parameters M_ϕ for different size square clusters are shown in Fig.6. Here M_ϕ is given by equation as below,

$$M_\varphi = \frac{1}{N}\sum_i \left(\mathbf{S}_i \times \frac{\mathbf{r}_i - \mathbf{r}_c}{|\mathbf{r}_i - \mathbf{r}_c|} \right)_z .$$ (3)

N represents total spin number and $\mathbf{r}_i$ and $\mathbf{r}_c$ are coordinate vectors of the spin $\mathbf{S}_i$ and the center of circle structure, respectively. Figure 6 shows M_ϕ increases as temperature decreases for the cluster with $L=75$ and 100.

Figure 7 shows the variation of normalized magnetization M and the closure domain structure parameter M_ϕ depending on size of square clusters with the one side length L. It is clearly seen that single domain structure turns to the closure domain structure accompanied with increasing of L.

As a result, the parallelized algorithm is available for the greater clusters including magnetic dipole interaction.
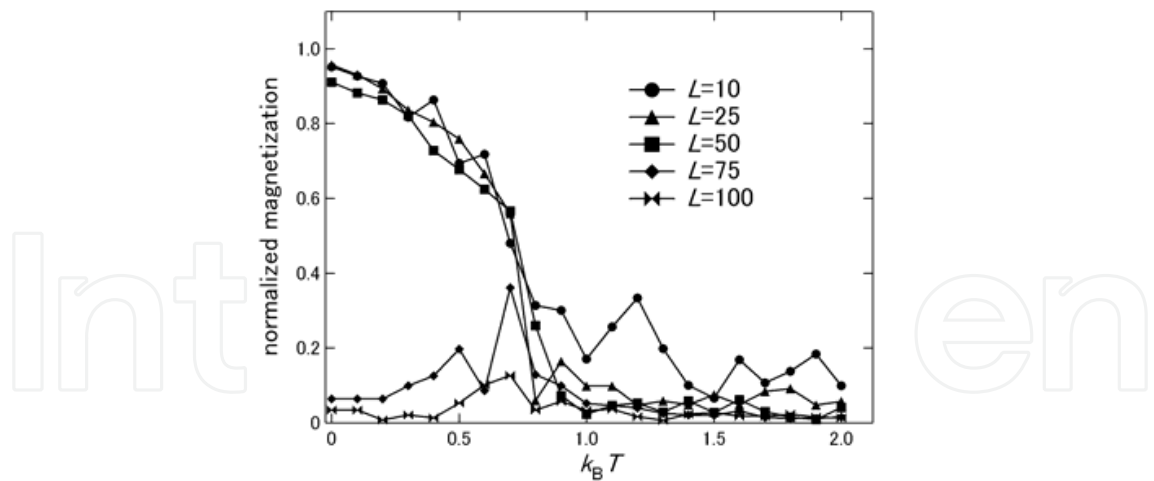
Fig. 5. Temperature dependence of normalized magnetization M for different size square clusters.
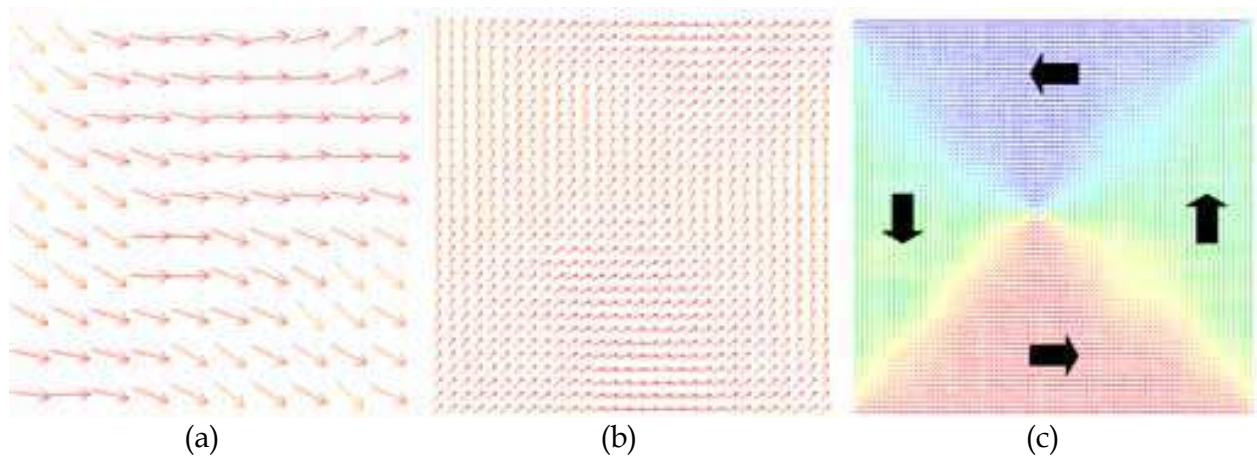

(a)   (b)   (c)

Fig. 6. Spin snapshots for different size square clusters with one side length of (a) L=10, (b) L=30, (c) L=75 at lowest temperature. Closure domain structure of spin system appears for L=75. Arrows on (c) represent directions of magnetic domains.
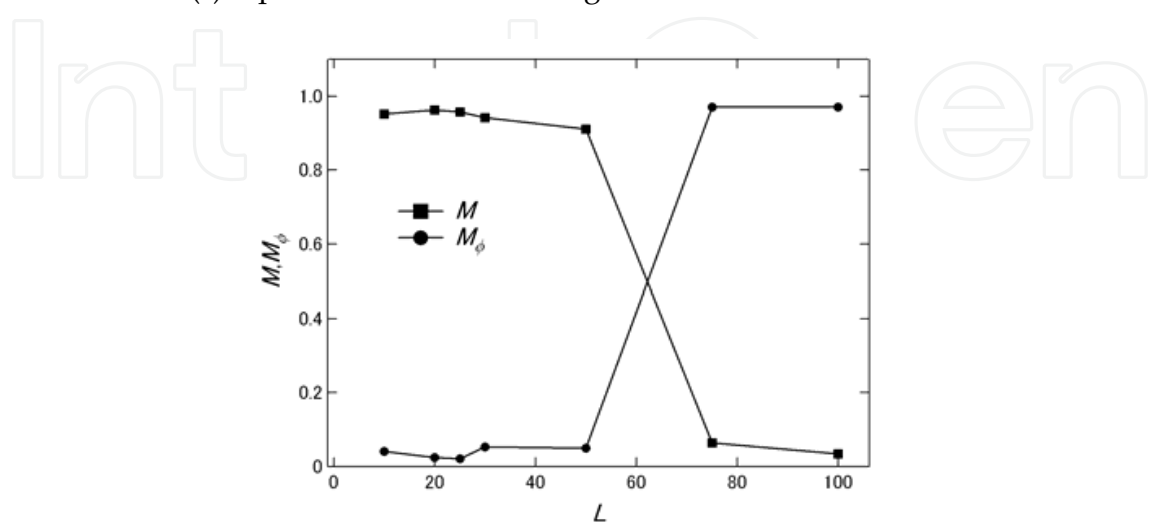

Fig. 7. Variation of M and M_ϕ depending on square cluster size with L.

Here, magnetic susceptibilities of Europium chalcogenides were simulated as a function of temperature for a concrete example to demonstrate the usefulness of the parallelized MC program. Europium chalcogenides, such as EuO, EuS, EuSe, EuTe, are typical ionic magnetic materials (Mauger & Godart 1986). The crystal structure has NaCl type and two types of the exchange energy exist; that is, J_1 for nearest site and J_2 for second nearest site. These exchange energies change depending on the lattice constants. Magnetic properties show ferro-magnetism for $|J_1| > |J_2|$ as EuO and antiferro-magnetism for $|J_1| < |J_2|$ as EuTe.
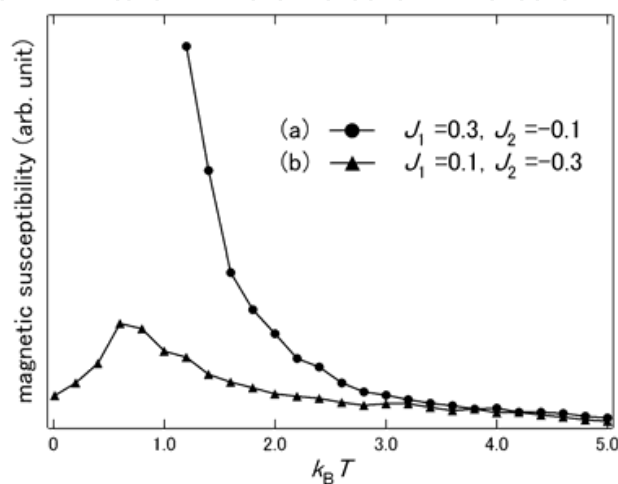
Fig. 8. Temperature dependence of magnetic susceptibilities of Europium chalcogenides for (a) $J1$=0.3, $J2$=-0.1 and (b) $J1$=0.1, $J2$=-0.3.
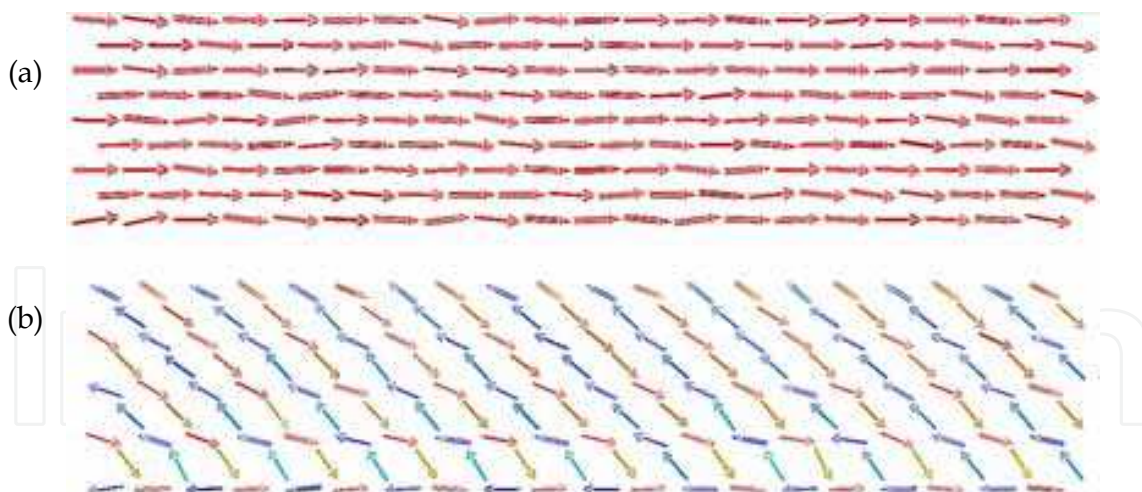
Fig. 9. Spin snapshots for a part of rectangular clusters of Eu chalcogenides with (a) $J1$=0.3, $J2$=-0.1 and (b) $J1$=0.1, $J2$=-0.3.

Relative exchange energies were set as (a) J_1=0.3, J_2=-0.1 and (b) J_1=0.1, J_2=-0.3 for a rectangular cluster with each side length of 5x5x50. These magnetic susceptibilities are estimated as gradients of the magnetization as a function of applied magnetic field B at each temperature. As shown in Fig. 8, the temperature dependence of magnetic susceptibilities has different behavior between (a) and (b). The susceptibility of (a) diverges around temperature k_BT=1.0 and the magnetic property shows ferro-magnetism. The direction of the

magnetization aligns toward a longitudinal direction of the cuboids cluster by magnetic dipole interaction at low temperatures as shown in Fig. 9(a). The susceptibility of (b), on the other hand, has a peak around k_BT=0.8 and the magnetic property shows antiferro-magnetism. Their spins align as anti-parallel as shown in Fig. 9(b).

For large magnetic cluster with many spins, the parallized MC method is very useful, although other MC method exists for huge clusters using FFT analysis (Sasaki & Matsubara 1997). The reason is that the parallized MC method can directly deal with complicated interactions without any average operations, such as plural exchange interactions due to different elements or local interactions due to impurities and voids which are important for studying magnetic properties of real materials.

4. Producing of magnetic domain

Magnetic domains in magnetic materials are produced by conflict among exchange interaction, magnetic dipole interaction and crystal anisotropy. In this section, using above MC method, the behavior of magnetic domains is represented. Here magnetic states were assumed that they depend on a Hamiltonian H including an exchange interaction energy H_J, a magnetic dipole interaction energy H_D, a magnetic anisotropy energy H_A and an applied magnetic field energy H_B;

$$H = H_J + H_D + H_A + H_B. \tag{4}$$

H_J term, H_D term and H_B term are same in Eq. (1). H_A term is given as following equations;

$$H_{A\_macro} = K_1 \sum_i \left(S_{i_x}^2 \cdot S_{i_y}^2 + S_{i_y}^2 \cdot S_{i_z}^2 + S_{i_z}^2 \cdot S_{i_x}^2 \right), \tag{5a}$$

$$H_{A\_micro} = A \sum_i \left(\frac{1}{\left| \mathbf{r}_{ij} - a_r \mathbf{S}_i \right|} - \frac{1}{\left| \mathbf{r}_{ij} \right|} \right). \tag{5b}$$

Equation (5a) is usual anisotropy representation for bcc crystal structure and Eq.(5b) is microscopic conventional anisotropy which was introduced to study for a deformed cluster. Below the parameters were set to J_{ij}=1.0, D=0.1, K_1=1.0, A=5 and a_r=0.3, respectively. These are tentative values to examine the usefulness of the model. The effective radius was set to r_{eff}=0.97 when excluding the second nearest neighbor spins in bcc structure.

Two spin systems of bcc structure with the lattice constant L=1 were formed into a cylindrical cluster with a diameter of 28L and 2L thickness including the number of 3291 spins and a spherical cluster with a diameter of 18L including the number of 7239 spins.

Figure 10 shows the temperature dependence of the closure domain structure parameter M_ϕ for the cylindrical cluster using each Hamiltonian; (a) $H_J + H_D$, (b) $H_J+H_D+H_{A\_macro}$, (c) $H_J+H_D+H_{A\_micro}$. Here M_ϕ is defined as same as Eq.(3);

Note that M_ϕ at the lowest temperature appears to be in the stable state, because it is the result after cooling down from sufficiently higher temperatures. Then the result without any anisotropies (a) shows M_ϕ=1.0, on the other hand, ones with anisotropies (b) and (c) show M_ϕ=0.95. The decreases of M_ϕ for the calculations with both anisotropies are due to producing magnetic domain walls (DWs). As shown in Fig.11(b), four divided magnetic domains were produced with 90 degree DWs (Neel walls); almost the spins align toward the

x-axis [100] and the y-axis [010], nevertheless the spin directions gradually change in Fig.11(a). When using $H_J+H_D+H_{A\_micro}$, the snapshot at the lowest temperature shows almost similar to Fig.11(b). As shown in Fig. 11, the effect of H_A is reflected in magnetic domain producing on a cylindrical cluster.
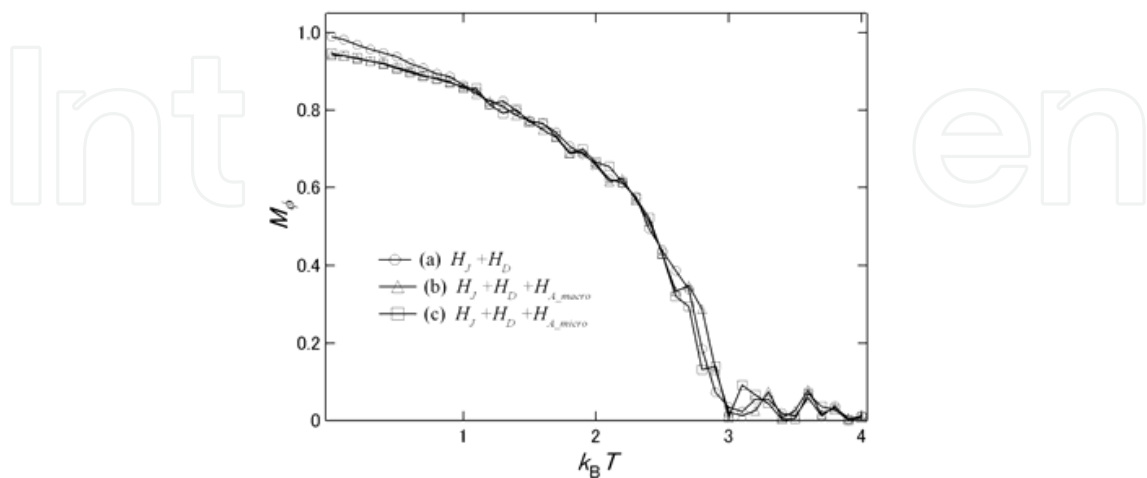

Fig. 10. Closure domain parameter M_ϕ as a function of temperature kBT for a cylindrical cluster using Hamiltonian; (a) $H_J+ H_D$, (b) $H_J+H_D+H_{A\_macro}$, (c) $H_J+H_D+H_{A\_micro}$.
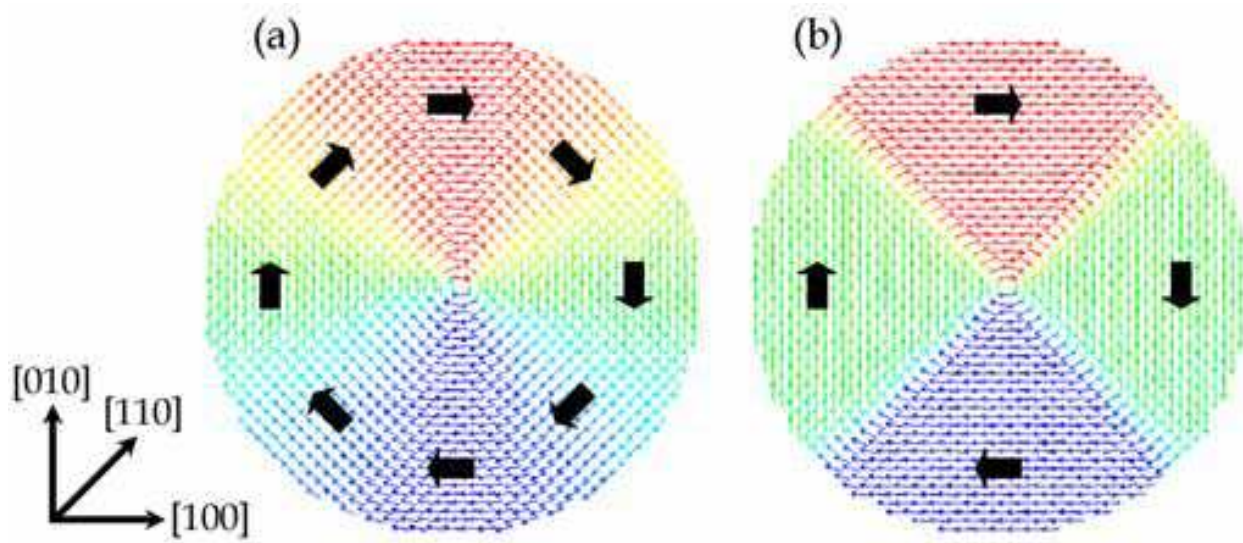
Fig. 11. Spin snapshots for a cylindrical cluster at the lowest temperature using Hamiltonian; (a) $H_J+ H_D$, (b) $H_J+H_D+H_{A\_macro}$.

Figure 11 shows the effect of H_A for magnetic domain producing in a cylindrical cluster. As shown in Fig. 11(b), four divided magnetic domains were produced with 90 degree domain walls (Neel walls); almost the spins align toward the x-axis [100] and the y-axis [010], nevertheless the spin directions gradually change in Fig. 11(a). When using $H_J+H_D+H_{A\_micro}$, the snapshot at the lowest temperature shows almost similar to Fig. 11(b).

Figure 12 shows magnetizations as a function of applied magnetic field (M-H curves) at the temperature of $k_BT=0.1$ along the [100] and [110] directions for the cylindrical cluster using $H_1=H_J+H_D+H_{A\_macro}+H_B$ including the macroscopic anisotropy and $H_2=H_J+H_D+H_{A\_micro}+H_B$

including the microscopic anisotropy. For both Hamiltonians, the anisotropy properties correspond qualitatively to the experimental result of bcc iron's one; the M-H curves show the magnetization along the [100] direction rapidly increases and reaches the saturated magnetization soon, and one along the [110] direction increases slowly on the way, therefore the [100] direction is the axis of easy magnetization for the cluster (Kittel 1986).
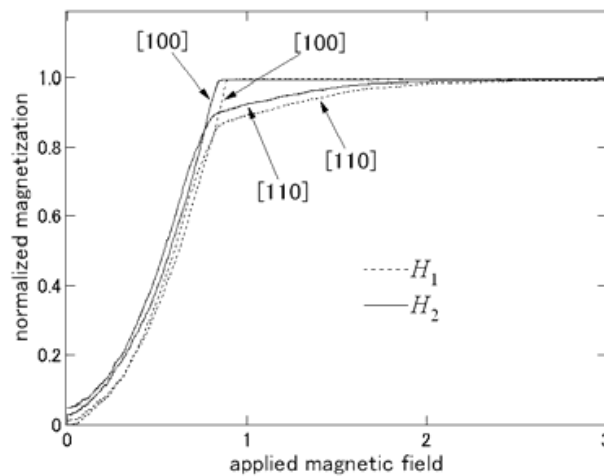

Fig. 12. Magnetizations as a function of applied magnetic field along the [100] and [110] directions for a cylindrical cluster using $H1 = H_J + H_D + H_{A\_macro} + H_B$ and $H2 = H_J + H_D + H_{A\_micro} + H_B$.

Figure 13 shows spin snapshots on the magnetization processes for the cylindrical cluster using H_2, when the magnetic field was applied along the [100] direction and the [110] direction. For the magnetic field along the [100] direction, DWs are monotonously moving and the magnetic domain including the spins toward the [100] direction in four divided magnetic domains gradually grow with increasing the magnetic field up to the saturation magnetization around $B=0.85$. On the other hand, for the magnetic field along the [110] direction, at first, two magnetic domains including the spins toward the [100] and the [010] directions grow and form one big DW at around $B=0.85$. Then the DW was fixed and the spins in the two domains gradually rotate toward the [110] direction, that is, rotation magnetization. In Fig.12, the slope of the M-H curve with the applied magnetic field along the [110] direction decreases more than around $B=0.8$ and the result depends on the slow reaction of the rotation magnetization with increasing magnetic fields.

Figure 14 shows M-H curves at the temperature of $k_B T = 0.1$ along the [100], [110] and [111] directions for the spherical cluster using H_1 and H_2. The results show the [111] direction is the axis of hard magnetization as similar as the experimental results of bcc iron (Kittel 1986). Above magnetic properties using H_2 as shown in Fig. 12, Fig. 13 and Fig. 14 well correspond to the results of the simulation using H_1. As a result, it would be possible to deal with H_2 as alternative to H_1. An advantage of H_2 including the microscopic anisotropy is to simulate magnetic processes for deformed clusters which have local crystal asymmetry.

Figure 15 shows spin snapshots on the magnetization processes for the original cylindrical cluster and the cylindrical cluster elongated 1.01 times along the [010] direction as a deformed cluster using H_2, when the magnetic field was applied along the [110] direction. Here the parameter A in (5b) is set to $A=10$ for more clearly checking the effect of the anisotropy. The results for the original cluster (left side in Fig. 15) are similar to ones in Fig.13 (right side). But the results for the deformed cluster, after the big DW produced by

the growth of two magnetic domains, the DW is still moving with rotation magnetization more than B=0.85, that is, the DWD has two steps process. The latter DWD would be regarded as the balance of pressure on DW broke due to asymmetric anisotropy in terms of "equation of motion for DW". But above model can introduce the DWD behavior naturally without importing other parameters.

The difference of the DWD behavior between the original cylindrical cluster and the deformed cluster does not clearly affect the M-H curves as shown in Fig. 16. This means the measurements of M-H curves could not give any efficient information for DWD. Then the other measurement such as Barkhauzen noise would be needed to more exactly know DWD behavior.

As mentioned above, MC simulations using H_2 including a microscopic anisotropy will be useful to study for DWD behavior, although now the results correspond to experimental one only qualitatively. H_{A_micro} in H_2 is originally introduced as crystal field from surrounding ligands, that is, a summation of Coulomb potentials. In general the charges in metals are strongly screened by conduction electrons. Therefore H_{A_micro} should be rather thought as a representation of a hybridization effect between electron wave functions, then the parameter A and a_r in H_{A_micro} would concern with the intensity of transfer integrals and the effective radius of the wave function respectively. As a result, the proposed model has a possibility to connect DWD behavior with material properties more deeply.
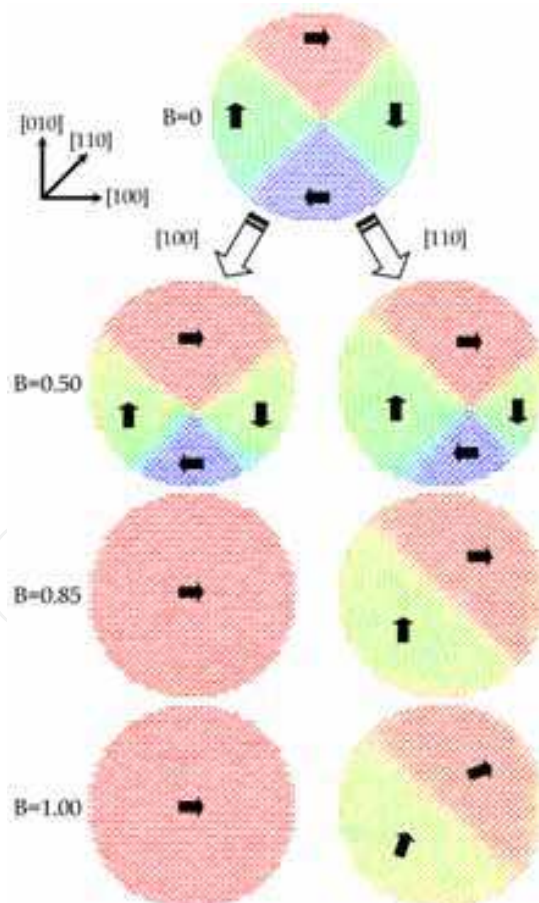

Fig. 13. Spin snapshots on magnetization processes for a cylindrical cluster using $H2= H_J+H_D+H_{A\_micro}+H_B$, when magnetic fields were applied along the [100] direction (left side) and along the [110] direction (right side).
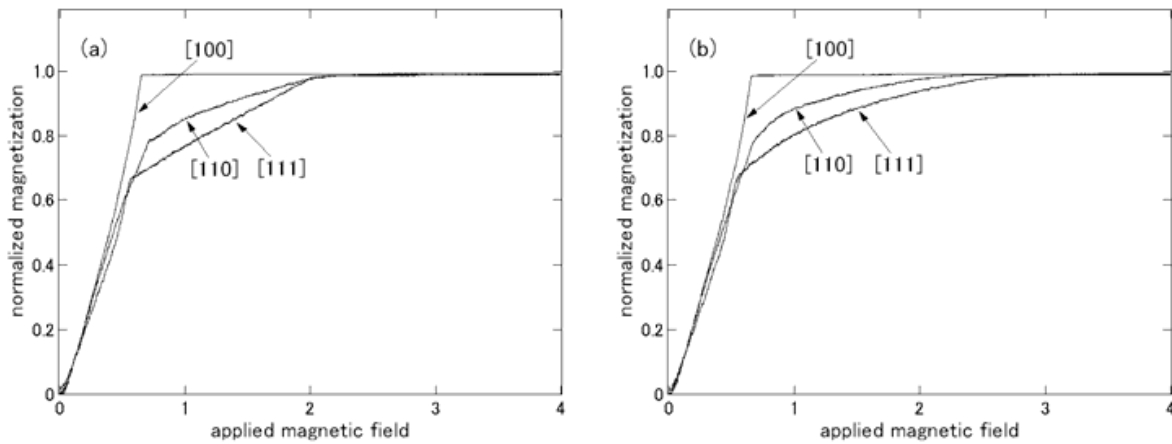
Fig. 14. Magnetization as a function of applied magnetic field along the [100], [110] and [111] directions for a spherical cluster using (a) $H1=H_J+H_D+H_{A\_macro}+H_B$ and (b) $H2=H_J+H_D+H_{A\_micro}+H_B$.
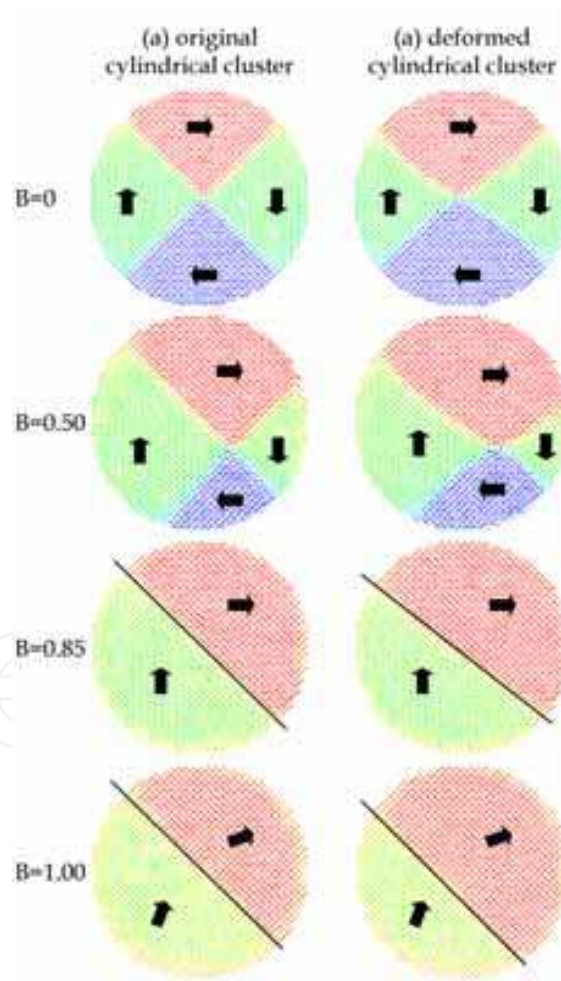

Fig. 15. Spin snapshots on magnetization processes for (a) the original cylindrical cluster and (b) the deformed cylindrical cluster elongated 1.01 times along the [010] direction, when magnetic fields were applied along the [110] direction. Note that parameter A in (4b) is set to A =10.
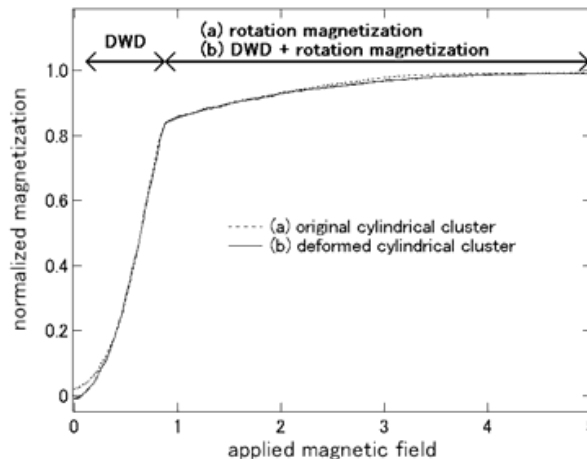
Fig. 16. Magnetizations as a function of applied magnetic fields along the [110] direction for (a) the original cylindrical cluster and (b) the deformed cylindrical cluster using $H2= H_J+H_D+H_{A\_micro}+H_B$. Note that parameter A in (4b) is set to $A =10$.

5. DWD for nano-wire

In this section, based on above method, the behavior of magnetic domain wall displacement (DWD) for nano-wire is simulated, which is important study for spintronics (Yamaguchi *et al*. 2009).

Here a rectangular solids spin system composed of 5x5x150 cells ($0 \leq x \leq 4$, $0 \leq y \leq 4$, $0 \leq z \leq 149$) standing for a nano-wire was prepared as a normal spin system without any local disorder. A following Hamiltonian was used for the simulation:

$$H = H_J + H_D + H_B$$
$$= -\sum_{near} J_{ij}\mathbf{S}_i \cdot \mathbf{S}_j + D\sum_{all}\left(\frac{\mathbf{S}_i \cdot \mathbf{S}_j}{|\mathbf{r}_{ij}|^3} - \frac{3}{|\mathbf{r}_{ij}|^5}\left(\mathbf{S}_i \cdot \mathbf{r}_{ij}\right)\left(\mathbf{S}_j \cdot \mathbf{r}_{ij}\right)\right) + B\sum_i \mathbf{S}_i . \tag{1}$$

In this simulation, the parameters were set as $J_{ij} =1.0$ between normal spins, $r_{eff} =1.0$, $D=0.1$. The value of $\mathbf{S}_i$ was fixed as $|\mathbf{S}_i| =1$. In this section, for simplicity, above Hamiltonian has no crystal anisotropy, although it has an important role for producing magnetic domains as shown in section 4. Here, alternatively, a shape magnetic anisotropy due to magnetic dipole interaction between spins produces magnetic domains.

Figure 17 shows temperature dependence of normalized magnetization M gradually cooling down from $k_BT=2.0$ to $k_BT=0.01$ for the rectangular cluster whose initial spin states were taken as random directions. Here M is defined as below

$$M = \frac{1}{N}\left|\sum_i \mathbf{S}_i\right|. \tag{6}$$

At each temperature, M is determined after N MCS repeating for producing the results in equilibrium. The curve obeys the Curie Weiss law and it has the Curie temperature of about $k_BT_c=1.5$. At the lowest temperature, almost spins align toward the longitudinal direction of the rectangular cluster due to the shape magnetic anisotropy as shown in Fig.18. Figure 19 shows applied magnetic field dependence of normalized magnetization M_z, that is,

magnetic hysteresis curve. The direction of magnetic field B is set to the axis of z and applied on the process $B = 0 \rightarrow +1.0 \rightarrow -1.0 \rightarrow +1.0$ with the step width $\Delta B=0.01$. Here, M_z is defined as below

$$M_z = \frac{1}{N}\sum_i \mathbf{S}_i \cdot \mathbf{k}. \tag{7}$$

Here, $\mathbf{k}$ is the unit vector along z-axis. The rectangular cluster has a large coecive force which would be due to the shape magnetic anisotropy. M_z is saturated under the magnetic field of B=0.5.
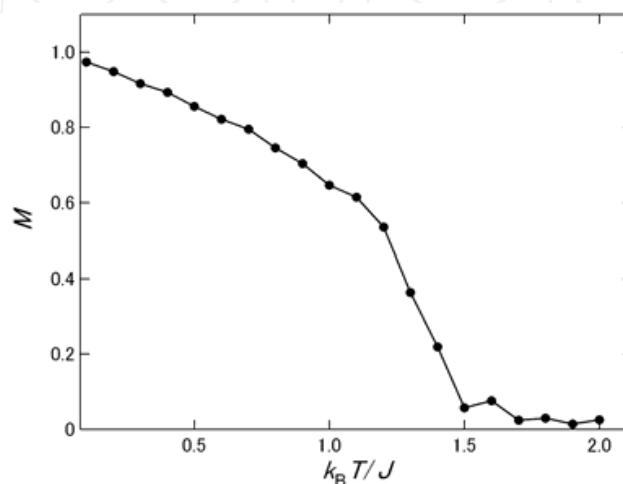
Fig. 17. Temperature dependence of normalized magnetization M for the rectangular cluster composed of 5x5x150 spins. M was simulated cooling down from higher temperatures.
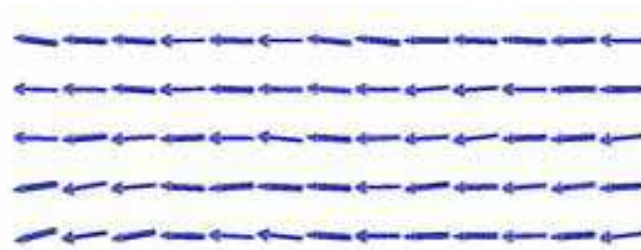
Fig. 18. Snapshot of the spin structure for the left edge of the rectangular cluster at the lowest temperature.

Next the constant reversal magnetic field of B=+0.5 was applied for the rectangular cluster with M_z=-1.0 at the lowest temperature in Fig. 17. Figure 20 shows the time dependence of M_z until 20000 MCS. The changing of M_z is small until 2500 MCS, and M_z changes with the almost constant gradient from 2500 MCS to 10000 MCS. Then M_z becomes constant over 10000 MCS, that is, saturation magnetization. The period until 2500 MCS is an initial step of the reversal magnetization process that spin directions were first reversed from sites around both longitudinal edge sides (z=0 and z=149) but obvious DWs are not produced yet. In the second period between 2500 and 10000 MCS, double DWs are produced around double edges of the rectangular cluster, as shown in Fig. 21(a), which shows a snapshot of the spin structure at t=3000 MCS. In the snapshot, there are double DWs at around z=10 and z=140 and the spins in the DWs take a screw structure, don't take Bloch or Neel typed DWs, as

shown in Fig. 21(b). Spin snap shots are shown in Fig. 21(c) on each MCS; 0 MCS, 3000 MCS, 6000 MCS and 10000 MCS.
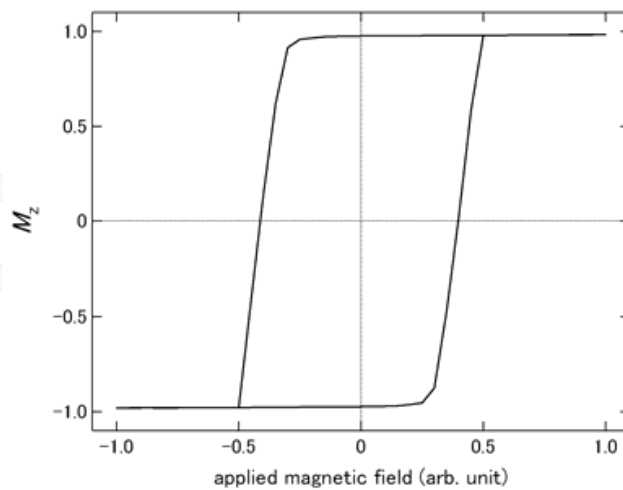

Fig. 19. Applied magnetic field dependence of Mz (hysiteresis curve) for the rectangular cluster with $Mz = -1.0$ at initial state.
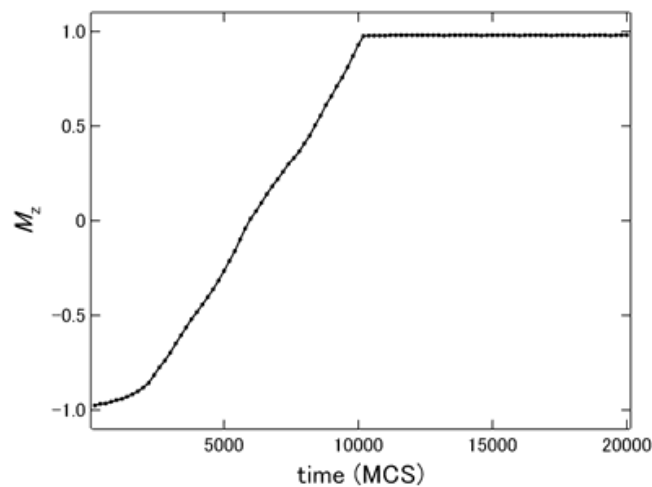

Fig. 20. Time dependence of Mz under the constant reversal magnetic field of $B = +0.5$ for the rectangular cluster with $Mz = -1.0$.

These DWs run toward the middle of the cluster until 10000 MCS as shown in Fig. 22. In this figure, each line shows an average of absolute value of the z component of spins ($=S_z$) included on the x-y plane at each z position at each increasing time elapse. Then each dip on line corresponds to the DW position, because S_z becomes smaller around DW than ones in other positions. In the last step, the double DWs vanish after encounter each other around the middle of the rectangular cluster over 10000 MCS.

Figure 23 shows the DW position depending on time elapses. In this model, using gradients of the DW position line for time, the DWD velocity was estimated as 0.93×10^{-2} (cell/MCS) for the rectangular cluster without impurities. Note that the velocity cannot be estimated by M_z in Fig.19, because the rectangular cluster has double DW on reversal magnetization process and the increasing of M_z is the result that the effects of double DWDs are superposed.

Here local disorders by magnetic impurities are introduced into the rectangular cluster as a normal spin system. These local disorders are randomly spread over the rectangular cluster until the number corresponding to the densities. Introducing of magnetic impurities is supposed to change no parameters of normal spins except for exchange interaction J_{ij}. The exchange interactions is set as $J_{ij} =1.5$ between a normal spin and an impurity, and $J_{ij} =2.0$ between impurities expecting magnetic enhancement due to the impurity.
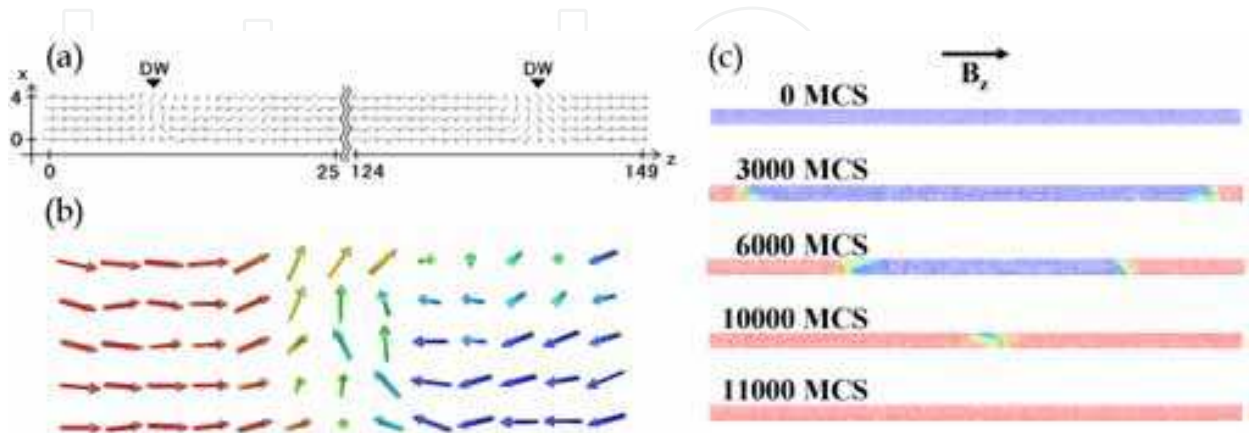
Fig. 21. (a) Snapshot of the spin structure during reversal magnetic field for the rectangular cluster at t=3000 MCS after the magnetic field was applied. (b) Enlarged view of snapshot of the spin structure around the left side DW in (a). (c) Spin snap shots on each MCS; 0 MCS, 3000 MCS, 6000 MCS and 10000 MCS.
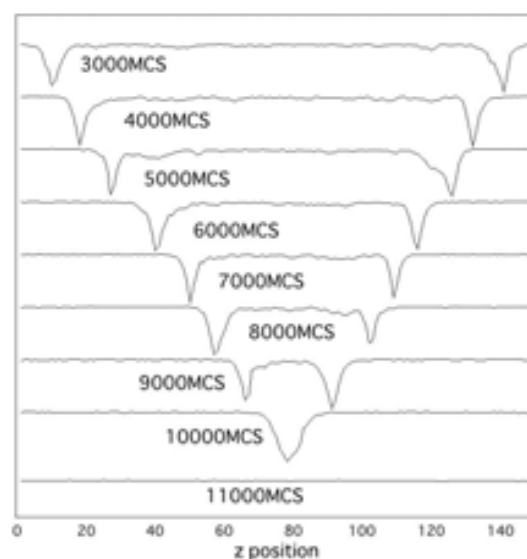
Fig. 22. Average of absolute value of Sz at each z position at each increasing time elapse, respectively. Each dip shows the DW position.

Figure 24 shows time dependence of DW position changes (ΔDWD) for the rectangular cluster with magnetic impurities, since obvious DW is produced under the reversal magnetic field. It is clearly seen that the gradients decrease with increasing the density of impurities.

Figure 25 shows variations of DWD velocity depending on impurities density. DWD velocity was found to decrease with increasing impurity.
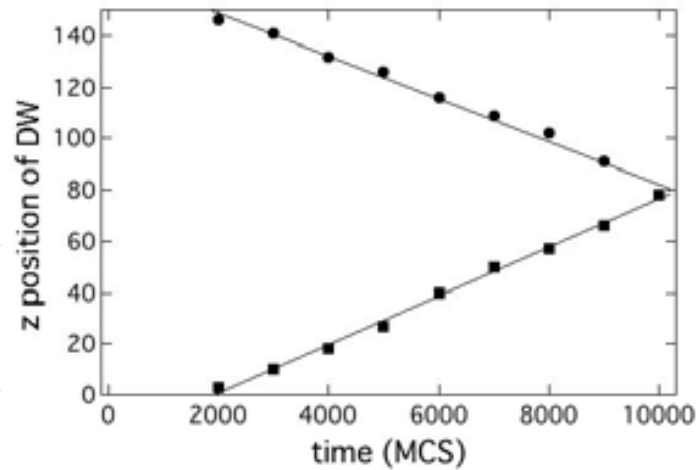
Fig. 23. Time dependence of the DW position on the left side (square markers) and right side (circle markers) of the rectangular cluster.
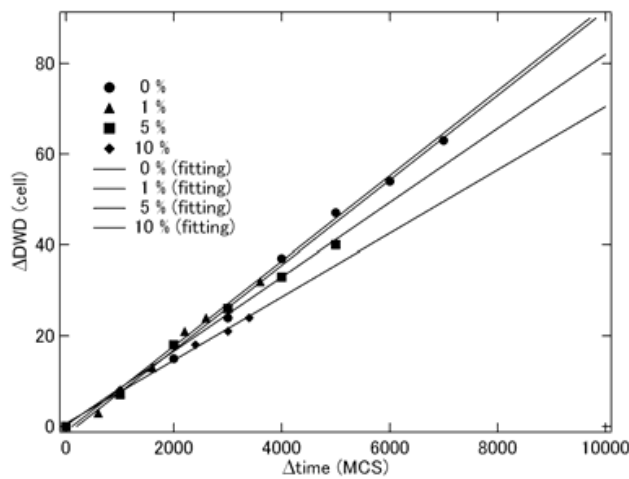

Fig. 24. Time dependence of the DW position changes of the rectangular cluster with various densities of magnetic impurities.
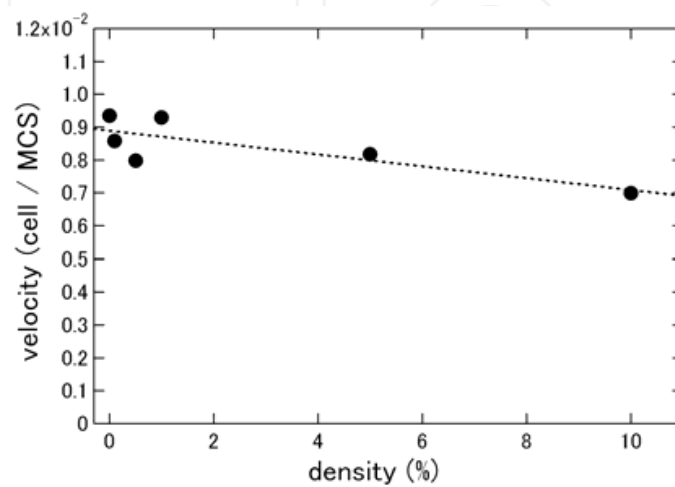

Fig. 25. DWD velocity changes with magnetic impurity densities.

In this section, DWD velocities were estimated for the rectangular clusters with different densities of magnetic impurities by MC simulation. The method above mentioned for investigating the behavior of DW will be useful for the development of nano-magnetic devices in near future.

6. M-H curves with a local magnetic distribution

The nickel-base superalloy Alloy 600 (Inconel) is widely used as structural materials for their high mechanical strength, e.g. for atomic power plants, and therefore early detection of the fatigue of the materials is very important. It is known that the sensitization of Alloy 600 due to chromium (Cr) depletion near the grain boundary by thermal heat treatment causes the integranular stress corrosion cracking (IGSCC), then especially the behavior under the sensitization has been studied as pressing matters (Kowaka *et al*. 1981, Wang & Gan 2001, Mayo 2004). It has been also known that the sensitization produced the magnetism in Alloy 600 which has no magnetism originally (Aspden *et al*. 1972, Takahashi *et al*. 2004b). Recently relationship between magnetic properties and sensitization is focused with expectation for potentiality of nondestructive evaluation (NDE) (Takahashi *et al*. 2004a). Several experimental reports show the magnetization occurs at Cr depletion areas around grain boundaries and the degree of sensitization affects the magnetic properties such as magnetic hysteresis (M-H) curves. But now it is not solved yet how the distribution of Cr depletion affects the change of magnetism in Alloy 600, although the relationship between the distribution of Cr depletion and the magnetism is important to estimate of the degree of sensitization using magnetic NDE.

In this section, magnetic properties of sensitized Alloy 600 by different heating duration times were simulated using Monte Carlo (MC) method and the results are discussed focusing on M-H curves affected by the sensitization (Yamaguchi *et al*. to be published).

A cubic system composed of 31^3 cells ($0 \leq x \leq 30$, $0 \leq y \leq 30$, $0 \leq z \leq 30$) was prepared including magnetic sites with a distribution. The distribution was decided by Cr depletion degree around a grain boundary on the supposition that Cr depletion introduces magnetic moments around the depletion area (Aspden *et al*. 1972, Takahashi *et al*. 2004b). The distribution of Cr depletion depending on heating duration time was calculated by thermodynamic analysis (Pruthi *et al*. 1977, Was & Kruger 1985, Grujicic & Tangrila 1991, Kai *et al*. 1993, Bao *et al*. 2006). Here the heating duration time means the period of thermal annealing under a constant heating temperature. Figure 26 shows the calculation results of the distributions of Cr depletion with each duration time (1h, 25h, 50h, 150h) under the heating temperature at 650 Celsius degree. The distributions of magnetic sites along x-axis of the cubic system corresponding to the distribution of Cr depletion are shown in Fig.27 as the surface view of the clusters. Here red circles represent the magnetic sites produced with a probability obeying the distribution of Cr depletion and blue circles are non magnetic sites. In Fig.27, the grain boundary is set on the y-z plane at the x-coordination of 15 and the edge surface coordination x=0 and x=30 are regarded as -300nm and +300nm in Fig.26 respectively.

A following Hamiltonian was used for the simulation:

$$H = H_J + H_D + H_B$$

$$= -\sum_{near} J_{ij} \mathbf{S}_i \cdot \mathbf{S}_j + D \sum_{all} \left(\frac{\mathbf{S}_i \cdot \mathbf{S}_j}{\left|\mathbf{r}_{ij}\right|^3} - \frac{3}{\left|\mathbf{r}_{ij}\right|^5} \left(\mathbf{S}_i \cdot \mathbf{r}_{ij}\right)\left(\mathbf{S}_j \cdot \mathbf{r}_{ij}\right) \right) + B \sum_i \mathbf{S}_i . \tag{1}$$

In this simulation, the parameters were set as J_{ij} =1.0, r_{eff} =1.0, D=0.01 in Eq.(1).
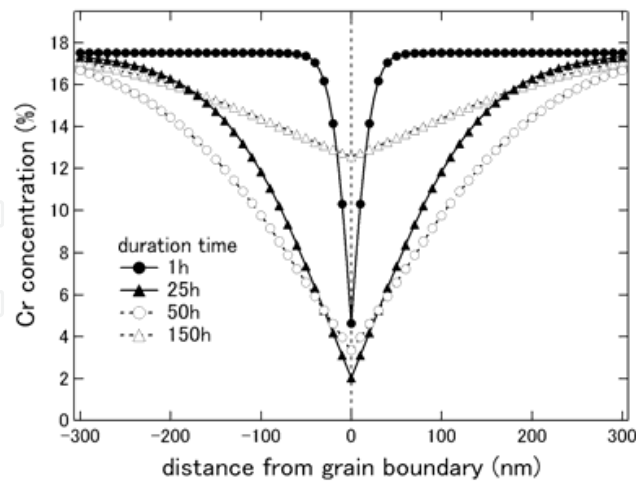

Fig. 26. Distribution of Cr depletion as a function of distance from grain boundary for each heating duration time.
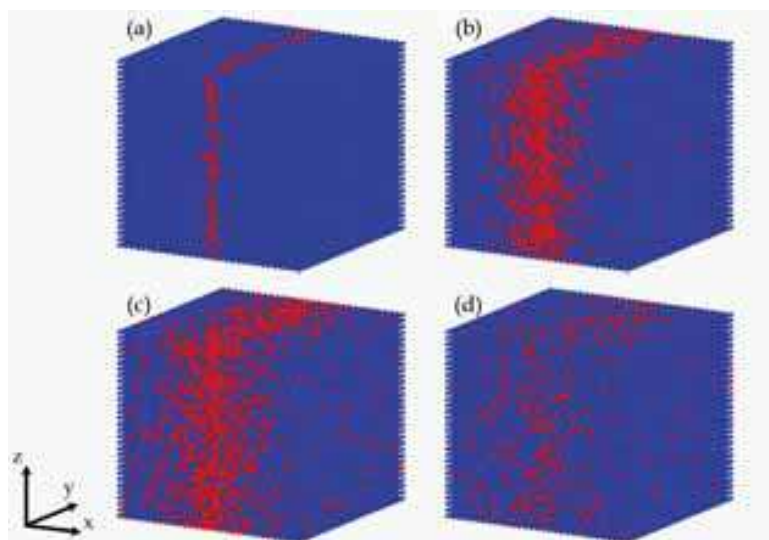

Fig. 27. Surface view of model clusters including magnetic sites due to the distribution of Cr depletion for duration time of (a) 1h, (b) 25h, (c) 50h and (d) 150h. Red circles and blue circles represent magnetic sites and non magnetic sites, respectively.

Figure 28(a) shows the experimental results of the magnetic M-H curves for Alloy 600 with different heating duration times. The measurements were performed at room temperature using vibration sample magnetometer (VSM). On the other hand, Fig. 28(b) shows the calculation results of M-H curves. The results of calculated M-H curves are the average of magnetization for two directions of applied magnetic field along perpendicular (x direction) and parallel (y direction) to grain boundary surface of cubic system, and the magnetization are normalized by total cell number (=31³). The applied magnetic field in this calculation is represented as arbitrary unit, and the value of 0.2 roughly corresponds to 2000 A/m in experiment from the estimation of magnetic field for saturation magnetization of the cluster with duration time of 50h. The behaviors of calculated M-H curves for duration times
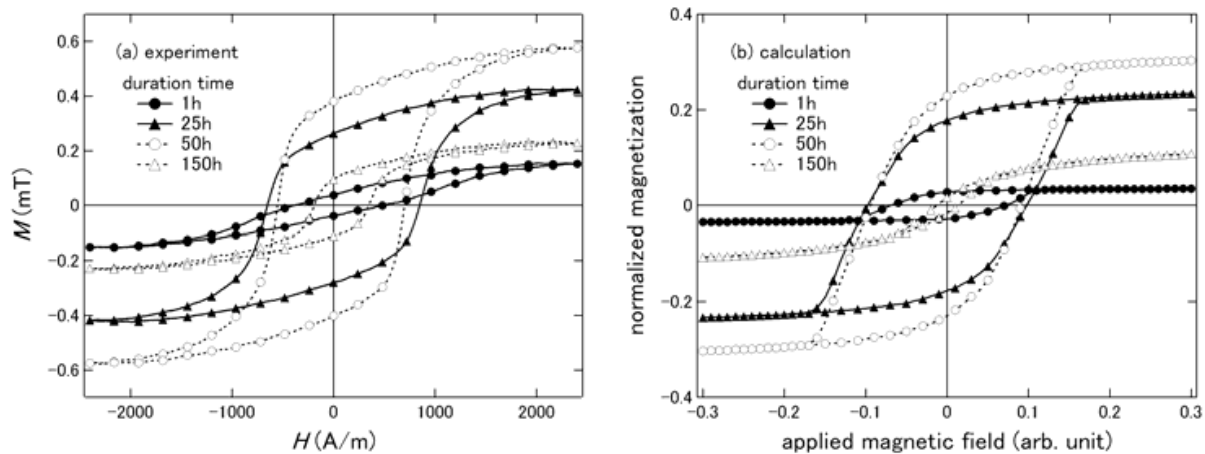
Fig. 28. M-H curves of (a) experiment and (b) calculation for each duration time.

correspond to the experimental ones, especially for the residual magnetization M_r and magnetic coercivity H_c which are important values in the demagnetizing curve.

Figure 29(a) and 29(b) show the heating duration time dependence of M_r and H_c, respectively, including more different duration times. The calculation result (solid line) has good correspondence with the experimental ones (dashed line). The difference of the duration time at M_r maximum between calculation and experiment can be due to the reliability of the estimated distribution of Cr depletion in Fig.26.
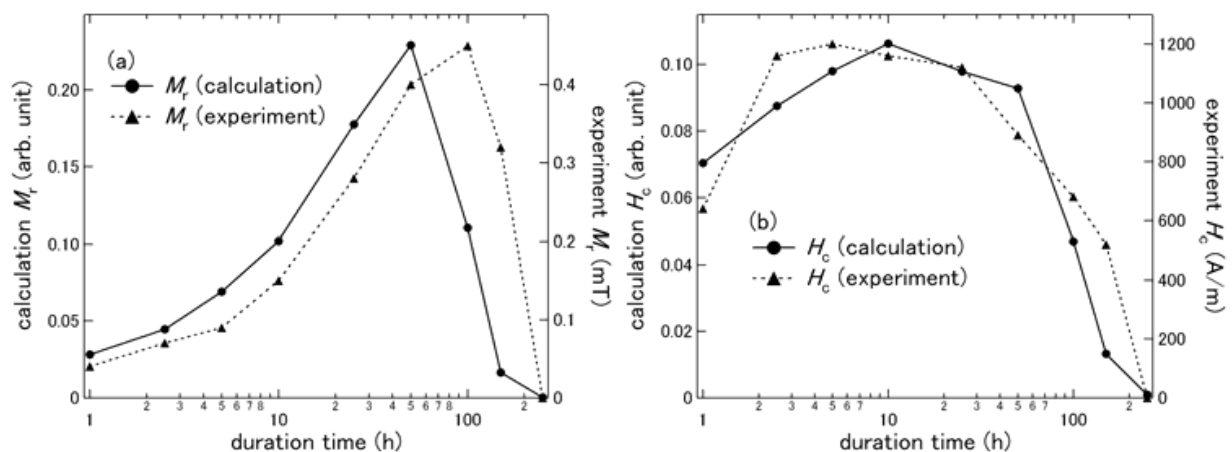
Fig. 29. Duration time dependence of (a) Mr and (b) Hc for experiment and calculation results.

To discuss focusing on the relationship between the distribution of magnetic site (= Cr depletion) and magnetic properties, such as M_r and H_c, the number of total magnetic sites in the cubic system and the average number of nearest neighbor magnetic sites are shown in Fig. 30(a) and 30(b), respectively as a function of the duration time. Here note the number of nearest neighbor magnetic sites for each magnetic site can range between 0 and 6, therefore the average number of nearest neighbor magnetic sites is different for each cluster corresponding to the distribution of Cr depletion as shown in Fig. 27. As shown in Fig. 29(a) and 30(a), M_r obeys the number of total magnetic sites. The result is reasonable in the view point that M_r is almost proportionate to the saturation magnetization. On the other hand, H_c nearly corresponds to the average number of nearest neighbor magnetic sites as shown in Fig. 29(b) and 30(b). In other words, H_c is affected by the density of magnetic sites around

grain boundary. Hence, these results suggest that the distribution of Cr depletion by sensitization, that is, the total amount of Cr depletion and the density of Cr depletion around grain boundaries can be estimated by M_r and H_c, respectively.

Above calculation model uses the exchange interaction with effective radius r_{eff} =1.0, then the effective strength of the exchange interaction depends on the number of the nearest neighbor magnetic sites. Now let us see the behavior of the effective interaction depending on the duration time in the view point of Curie temperature T_c which depends on the exchange interaction.

Figure 31 shows the temperature dependence of calculated magnetization without applied magnetic field for different duration times. The temperature below which the spontaneous magnetization appears, that is, T_c is depending on each duration time. To estimate T_c more exactly, temperature dependence of magnetic susceptibility χ is calculated by M-H curve for each temperature such as shown in Fig. 32. Figure 33 shows the temperature dependence of $1/\chi$ and T_c is estimated as the cross point of the temperature axis. Then the duration time dependence of T_c is also following the average number of the nearest magnetic sites as shown in Fig.34. The result suggests the effective exchange interaction affects both H_c and T_c through the density of magnetic sites due to Cr depletion around grain boundaries.
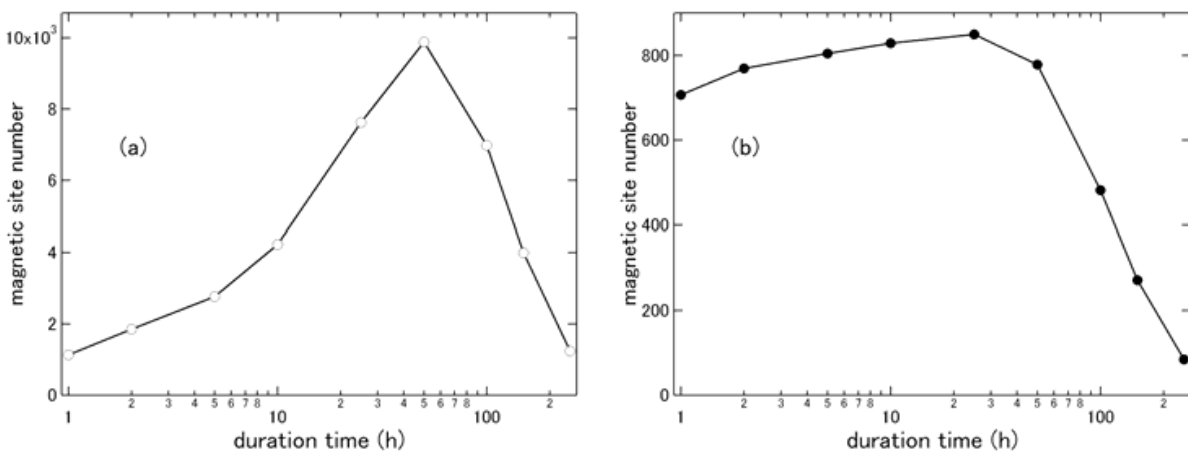

Fig. 30. Duration time dependence of (a) number of total magnetic sites and (b) average number of the nearest neighbor magnetic sites.
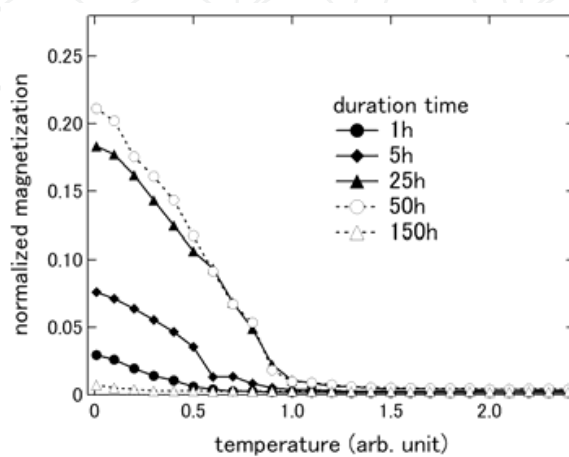

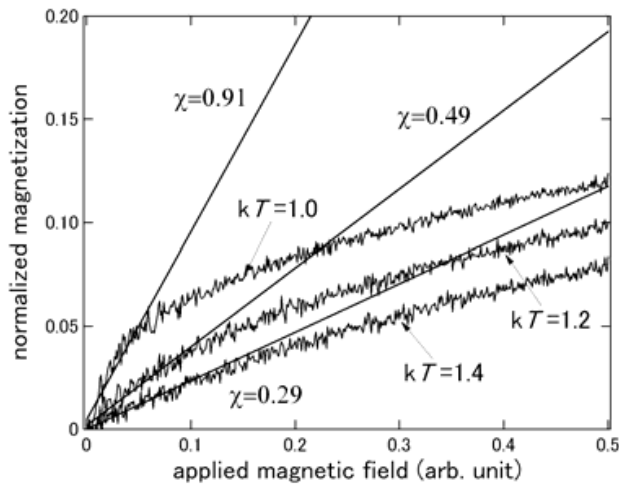Fig. 31. Temperature dependence of calculated magnetization for each duration time

Fig. 32. Example of calculation for magnetic susceptibility χ from M-H curve at each temperature for the duration time of 25h.
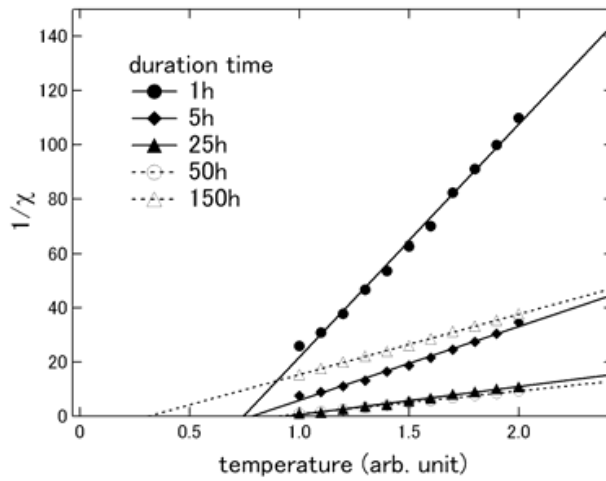

Fig. 33. Temperature dependence of inverse of calculated magnetic susceptibility $1/\chi$ for each duration time.
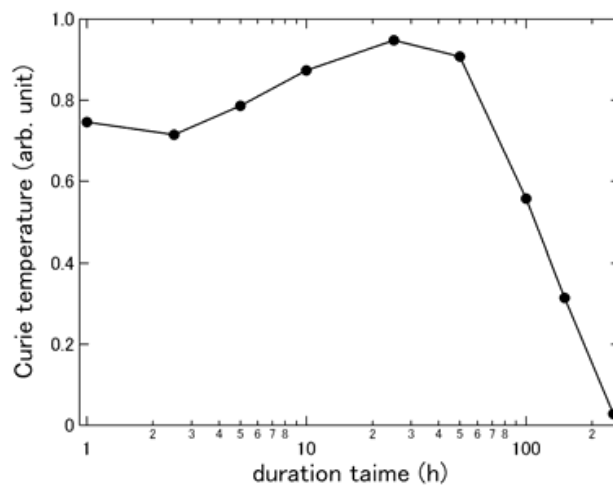

Fig. 34. Duration time dependence of Curie temperature.

In above the model, magnetic particles due to Cr depletion disperse around a grain boundary in Alloy 600 and it can be regarded as a magnetic granular structure with a distribution. Then M_r and H_c on a M-H curve tell the total amount and the density of Cr depletion around grain boundaries, respectively. Therefore the analysis of magnetic dynamic process using Monte Carlo method would tell the degree of sensitization due to fatigue for Alloy 600.

7. References

Aspden, R. G.; Economy, G.; Pement, F. W. & Wilson, I. L. (1972). Relationship Between Magnetic Properties, Sensitization, and Corrosion of Incoloy Alloy 800 and Inconel Alloy 600. *Metallurgical Transactions*, Vol. 3, 2691-2697

Bao, G.; Shinozaki, K.; Inkyo, M.; Miyoshi, T.; Yamamoto, M.; Mahara, Y. & Watanabe, H. (2006). Modeling of precipitation and Cr depletion profiles of Inconel 600 during heat treatments and LSM procedure. *Journal of Alloys and Compounds*, Vol. 419, No.1-2, August , 118-125

Grujicic, M. & Tangrila, S. (1991). Thermodynamic and kinetic analyses of time-temperature-sensitization diagrams in austenitic stainless steels. *Materials Science and Engineering*, Vol.A142, No.2, August, 255-259

Kai, J. J.; Tsai, C. H. & Yu, G. P. (1993). The IGSCC, sensitization, and microstructure study of Alloys 600 and 690*. *Nuclear Engineering and Design*, vol. 144, No.3, November, 449-457

Kittel, C. (1986). *Introduction to Solid State Physics, 6th ed.*, John Wiley & Sons, Inc., ISBN, New York

Kowaka, M.; Nagano, H.; Kudo, T. & Okada, Y. (1981). Effect of Heat Treatment on The Susceptibility To Stress Corrosion Cracking of Alloy 600. *Nuclear Technology*, Vol. 55, 394-404

Landau, D. P. & Binder, K. (2000). *A Guide to Monte Carlo Simulations in Statistical Physics*, Cambridge University Press, 0521653665, Cambridge

Mauger, A. & Godart, C. (1986). The magnetic, optical, and transport properties of representatives of a class of magnetic semiconductors: The Europium chalcogenides. *Phys. Rep.*, Vol. 141, No.2-3, 51-176

Mayo, W. E. (2004). Predicting IGSCC/IGA susceptibility of Ni-Cr-Fe alloys by modeling of grain boundary chromium depletion. Materials Science and Engineering A, Vol.232, No.1-2, 129-139

Metropolis, N.; Rosenbluth, A.; Rosenbluth, M. & Teller, A. (1953). Equation of State Calculations by Fast Computing Machines. *J. Chem. Phys.*, Vol.21, No.6, 1087-1092

Pruthi, D. D.; Anand, M. S. & Agarwala, R. P. (1977). Diffusion of Chromium in Inconel-600. *Journal of Nuclear Material*, Vol. 64, No.1-2, January, 206-210

Sasaki, J. & Matsubara, F. (1997). Circular phase of a two-dimensional ferromagnet with dipolar interaction. *J. Phys. Soc. Jpn*, Vol.66, No.7, 2138-2146, 00319015

Takahashi, S.; Sato, H.; Kamada, Y.; Ara, K. & Kikuchi, H. (2004a). A new magnetic NDE method in inconel 600 alloy, IOS Press, Vol. 19, 3-8

Takahashi, S.; Sato, Y.; Kamada, Y. & Abe, T. (2004b). Study of chromium depletion by magnetic method in Ni-based alloys. *Journal of Magnetism and Magnetic Materials*, Vol. 269, 139-149

Vedmedenko, E. Y.; Oepen, H. P.; Ghazali, A.; Levy, J. C. S. & Kirschner, J. (2000). Magnetic Microstructure of the Spin Reorientation Transition: Computer Experiment. *Phys.Rev.Lett.*, Vol.84, No.25, 5884-5887

Wang, J. D. & Gan, D. (2001). Effects of grain boundary carbides on the mechanical properties of Inconel 600. *Materials Chemistry and Physics*, Vol. 70, No.2, 124-128

Was, G. S. & Kruger, R. M. (1985). A thermodynamic and kinetic basis for understanding chromium depletion in Ni-Cr-Fe alloys. *Acta Metallurgica*, Vol. 33, No.5, May, 841-854

Yamaguchi, K.; Tanaka, S.; Nittono, O.; Takagi, T. & Yamada, K. (2004). Monte Carlo simulation of dynamic magnetic processes for spin system with local defects. *Physica B*, Vol. 343, No.1-4, January, 298-302

Yamaguchi, K.; Suzuki, K.; Nittono, O.; Yamada, K.; Enokizono, M. & Takagi, T. (2009). Monte Carlo Simulation for Magnetic Domain Wall Displacements in Magnetic Nano-Wires with Local Disorders. *IEEE Trans. Magn.*, Vol. 45, No.3, March, 1622-1625

Yamaguchi, K.; Suzuki, K.; Nittono,; Uchimoto, T. & Takagi, T. (to be published). Magnetic Dynamic Process of Magnetic Layers around Grain Boundary for Sensitized Alloy 600. *IEEE Trans. Magn.*.
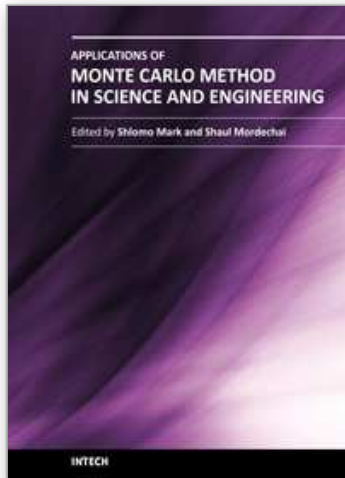
Applications of Monte Carlo Method in Science and Engineering

Edited by Prof. Shaul Mordechai

In this book, Applications of Monte Carlo Method in Science and Engineering, we further expose the broad range of applications of Monte Carlo simulation in the fields of Quantum Physics, Statistical Physics, Reliability, Medical Physics, Polycrystalline Materials, Ising Model, Chemistry, Agriculture, Food Processing, X-ray Imaging, Electron Dynamics in Doped Semiconductors, Metallurgy, Remote Sensing and much more diverse topics. The book chapters included in this volume clearly reflect the current scientific importance of Monte Carlo techniques in various fields of research.

How to reference

In order to correctly reference this scholarly work, feel free to copy and paste the following:

Katsuhiko Yamaguchi, Kenji Suzuki and Osamu Nittono (2011). Monte Carlo Simulation for Magnetic Domain Structure and Hysteresis Properties, Applications of Monte Carlo Method in Science and Engineering, Prof. Shaul Mordechai (Ed.), ISBN: 978-953-307-691-1, InTech, Available from:
http://www.intechopen.com/books/applications-of-monte-carlo-method-in-science-and-engineering/monte-carlo-simulation-for-magnetic-domain-structure-and-hysteresis-properties

INTECH
open science | open minds